Science of the Total Environment 823 (2022) 153649

Contents lists available at ScienceDirect

Science of the Total Environment

journal homepage: www.elsevier.com/locate/scitotenv

Smog chamber simulation on heterogeneous reaction of O_3 and NO_2 on black carbon under various relative humidity conditions

Si Zhang [a], Xinbei Xu [a], Yali Lei [a], Dapeng Li [a], Yiqian Wang [a], Shijie Liu [a], Can Wu [a], Shuangshuang Ge [b], Gehui Wang [a,c,*]

[a] Key Lab of Geographic Information Science of the Ministry of Education, School of Geographic Sciences, East China Normal University, Shanghai 200241, China
[b] Institute of Urban Meteorology, China Meteorological Administration, Beijing 100089, China
[c] Institute of Eco-Chongming, Chenjia Zhen, Chongming, Shanghai 202162, China

HIGHLIGHTS

- HNO_3 can be formed quickly from the hydrolysis of N_2O_5 on BC and then neutralized by NH_3 as NH_4NO_3.
- O_3 and NO_2 showed a synergetic oxidizing effect on BC and significantly activated the BC surface.
- The nitrate formation was enhanced under high RH conditions especially for KCl-containing BC particles.

GRAPHICAL ABSTRACT

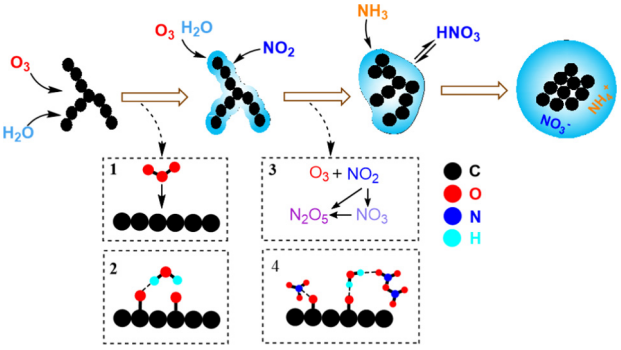

ARTICLE INFO

Article history:
Received 11 November 2021
Received in revised form 29 January 2022
Accepted 30 January 2022
Available online 11 February 2022

Editor: Pingqing Fu

Keywords:
Ammonia
Nitrate
N_2O_5
Synergetic oxidation
Formation mechanism

ABSTRACT

In this study, heterogeneous formation of nitrate from O_3 reaction with NO_2 on black carbon (BC) and KCl-treated BC surface in the presence of NH_3 was simulated under 30–90% RH conditions by using a laboratory smog chamber. We found that O_3 and NO_2 in the chamber quickly reacted into N_2O_5 in the gas phase, which subsequently hydrolyzed into HNO_3 and further neutralized with NH_3 into NH_4NO_3 on the BC surface, along with a small amount of N_2O_5 decomposed into NO and NO_2 through a reaction with the BC surface active site. Meanwhile, the fractal BC aggregates restructured and condensed to spherical particles during the NH_4NO_3 coating process. Compared to that during the exposure to NO_2 or O_3 alone, the presence of strong signals of CH_2O^+, $CH_2O_2^+$ and CH_4NO^+ during the simultaneous exposure to both NO_2 and O_3 suggested a synergetic oxidizing effect of NO_2 and O_3, which significantly activated the BC surface by forming carbonyl, carboxylic and nitro groups, promoted the adsorption of water vapor onto the BC surface and enhanced the NH_4NO_3 formation. Under <75 ± 2% RH conditions the coating process of NH_4NO_3 on the BC surface consisted of a diffusion of N_2O_5 onto the surface and a subsequent hydrolysis, due to the limited number of water molecules adsorbed. However, under 90 ± 2% RH conditions N_2O_5 directly hydrolyzed on the aqueous phase of the BC surface due to the multilayer water molecules adsorbed, which caused an instant NH_4NO_3 formation on the surface without any delay. The coating rate of NH_4NO_3 on KCl-treated BC particles was 3–4 times faster than that on the pure BC particles at the initial stage, indicating an increasing formation of NH_4NO_3, mainly due to an enhanced hygroscopicity of BC by KCl salts.

* Corresponding author at: Key Lab of Geographic Information Science of the Ministry of Education, School of Geographic Sciences, East China Normal University, Shanghai 200241, China.
E-mail address: ghwang@geo.ecnu.edu.cn (G. Wang).

http://dx.doi.org/10.1016/j.scitotenv.2022.153649
0048-9697/© 2022 Elsevier B.V. All rights reserved.

1. Introduction

Black carbon (BC) in the atmosphere is a type of carbonaceous aerosols and also named as soot, which is released directly from incomplete combustion of carbon-containing materials, and composed of many small spherical soot particles that collide with each other and coalesce to form aggregates with a chain or branched structure (Nie et al., 2020; Wei et al., 2020). BC ubiquitously exists from the ground surface to the stratosphere. In the past decades global annual emission of BC has continuously increased from 1957 Gg in 2007 to 2534 Gg in 2014 due to an increasing consumption demand for fossil fuels (Hoesly et al., 2018; Wang et al., 2012). Because of the significant impact on the atmospheric radiative forcing by absorbing solar radiation and facilitating water evaporation and cloud dissipation, BC has been taken by the IPCC report as the second most important anthropogenic global warming species (He et al., 2015; IPCC, 2013; Liao and Shang, 2015). In addition, BC particles are very tiny and can penetrate deeply into the lung and accumulate in human organs (Ban-Weiss et al., 2009), thus it is listed by WHO as a carcinogen.

Nascent BC particles are hydrophobic and chemically inert, but once emitted into the atmosphere they can undergo aging process, leading to changes in BC physicochemical properties (Guan et al., 2017; Jiang et al., 2019). Many papers reported that BC can provide surface for heterogeneous reactions of O_3, NO_2, volatile organic compounds (VOC) and other gas pollutants to occur. Moreover, secondary products can also condense on the BC surface and form a coating, which could change BC optical properties and hygroscopicity significantly (Zhang et al., 2020a; Leung et al., 2017a; Peebles et al., 2011). NOx and BC are the co-byproducts released from fossil fuels and biomass combustion process. Reactions of NOx and HNO_3 on BC surface have been widely studied (Saathoff et al., 2001; Zelenov et al., 2016). For example, Longfellow et al. (2000) examined the uptakes of HNO_3 and N_2O_5 on BC, and found that the uptake of HNO_3 was reversible and no NO_2 or NO was formed, while the uptake of N_2O_5 on BC was reactive and gas phase NO_2 was observed. However, under certain conditions, the heterogeneous conversion of NO_2 and NO from HNO_3 on BC can be produced. For an example, Kleffmann and Wiesen (2005) found that the formation of NO and NO_2 was observed only for high HNO_3 level (> 800 ppb), yet reversible adsorption was observed for HNO_3 < 600 ppb. In addition, HNO_3 also immediately decomposes on BC surface at 503 K even at lower HNO_3 level (Choi and Leu, 1998). Different BC can also affect the reactivity of HNO_3. Choi and Leu (1998) found that HNO_3 decomposed to NOx and H_2O on a commercial BC (Degussa FW2), while the phenomenon was much smaller on graphite and was not observed on hexane soot. These results showed that the mechanisms and dynamic characteristics of the heterogeneous reactions of NOx and related nitrogen oxides including HNO_3 on the BC surface are dependent on many factors such as reactant concentrations and BC properties itself.

In the last decade, atmospheric $PM_{2.5}$ and SO_2 levels reduced by about 50% in China due to the strict emission controls (Zhang et al., 2020b). However, VOCs and NOx levels in the country have not changed significantly, resulting in an increasing O_3 level in many Chinese urban regions (Li et al., 2019). A recent field observation reported that O_3 and NO_2 could abundantly co-exists in Chinese cities even in nighttime, causing a rapid formation of nitrate through producing N_2O_5 and its subsequent hydrolysis on airborne particles including BC (Wu et al., 2019). However, up to now the heterogeneous reaction of O_3 with NO_2 on BC surface has not been studied and the relevant mechanism is not clear especially under humid conditions. In this study, we investigated the heterogeneous reaction process of O_3 with NO_2 on BC particles by using a home-made smog chamber under various relative humidity (RH) conditions. To reveal the reaction mechanism of O_3 and NO_2 on BC surface, the change of reactant levels, the formation amount of nitrate, and size and morphology of BC particles were characterized, along with a comparison on the formation rate of nitrate under different RH conditions. Our results revealed an important synergistic effect of O_3 with NO_2, causing a rapid nitrate formation on the BC surface.

2. Experimental section

2.1. Methods

In this study, a Teflon smog chamber with a volume of 1.13 m^3 was used to conduct the simulation experiments (Fig. S1). All the experiments were carried out under dark conditions with a black cloth hood covering the chamber. The initial conditions of the experiments are given in the supplementary (Table S1). The experiment details were reported in our previous paper (Ge et al., 2019). Here we only give a brief description.

The simulation experiments were conducted under various RH (30–90%) conditions by exposing two types of seeds (i.e., BC and KCl-treated BC) to O_3 and NO_2, respectively. Zero air was used in the chamber as the background gas, which was formed through a Zero Air Supplier (model 111, Thermo scientific, USA). A commercial carbon black Regal 400 (R400, Cabot Corporation, USA) was selected as BC seeds. To mimic the biomass burning emitted BC aging process, a mixture suspension of the Regal BC and KCl with a mass ratio of 3:1 was used in this study, which is consistent with that in biomass burning plume observed in North China (Wang et al., 2020). The seed particles in this study were produced by using a home-made single jet atomizer through nebulizing the BC suspension or BC-KCl mixture suspension, respectively. Before each experiment, the chamber was flushed by the zero air about ten times until the concentrations of particle and gases inside the chamber were all below the instrument detection limits. The particles were dried by a Nafion dryer and charge neutralized by a soft X-Ray neutralizer (3088, TSI, USA), then a monodisperse mode of particles with a specific diameter were selected by a Differential Mobility Analyzer (DMA, 3081, TSI, USA) and introduced into the smog chamber for reaction. The size distribution of BC seeds in the chamber displayed a normal distribution with 117 nm mode size and 130 nm geometric mean size; while the size distribution of KCl-treated BC particles in the chamber exhibited 130 nm mode size and 134 nm geometric mean size, respectively. Ozone was produced by ultraviolet irradiation of pure oxygen with a 254 nm UV lamp (ZW23015Y-Z436, Cnlight, China). NO_2 (g) and NH_3 (g) reactant gases (Air Liquid Holding Company, China) were introduced into the chamber by using a glass syringe. The three gasses were injected sequentially into the smog chamber and each was introduced in one injection. Relative humidity inside the chamber was adjusted by a flow of humid air by bubbling the zero air through a bottle filled with ultrapure water (Milli Q, 18.2 MΩ, Millipore Company, USA) to the designed RH. All the experiments were performed under 298 K and 1 atm conditions (Fig. S1). Every experiment was conducted at least three times to ensure the accuracy of the results.

2.2. Gas and particle measurements

During the experiment process NO_2 were measured by using a Thermo Scientific NO_X Analyzer (Model 42i, Thermo scientific, USA). Particle mobility distribution was determined by Scanning Mobility Particle Sizer (SMPS, 3082, TSI, USA). In this study, the change of particle mass before and after reaction was detected by a tandem DMA, centrifugal particle mass analyzer (CPMA, 015-102, Cambustion, UK) and condensation particle counter (CPC, 3775, TSI, USA). During the detection, particles from the chamber were sent to the neutralizer and selected by DMA with a specific mode size, then measured by the CPMA for the mass of these monodisperse particles, and eventually counted by the CPC to obtain the particle number. The effective density (ρ_{eff}) and mass-mobility exponent (D_m) of particle can be calculated according to the mobility diameter and mass of the monodisperse particles in the above process by using the formulas below (Schnitzler et al., 2014):

$$\rho_{eff} = \frac{6m_p}{\pi d_m^3} \quad \text{(I)}$$

$$m_p = C d_m^{D_m} \quad \text{(II)}$$

Where m_p is the particle mass, d_m is the particle mobility diameter, and C is a constant.

Seeded particles in the chamber were collected onto copper TEM grids, which are coated with carbon film, by using a cascade impactor equipped with a 0.3 mm diameter jet nozzle under an air flow rate of 1.0 L/min condition (Li et al., 2021). Morphology and element distribution of the seeded particles were analyzed using a Transmission Emission Mirror (TEM, JEM-2100F, Japan), which was performed at 200 kV with X-ray energy diffraction (TEM/EDS). Chemical compositions of seeded particles were determined with a high-resolution time-of-flight aerosol mass spectrometer (HR-ToF-AMS, Aerodyne Research, USA). The detail information about the instrumentations used in this work can be found in Supplementary.

3. Results and discussion

3.1. Reaction mechanism of O_3 and NO_2 on BC surface

To clarify the reaction mechanism of O_3 and NO_2 on BC surface, BC particles with a diameter of 117 ± 1.31 nm were exposed consecutively to 300 ppb O_3 and 300 ppb NO_2 under 75 ± 2% RH conditions for 50 min in the presence of 500 ppb NH_3. As shown in Fig. 1a and b, in the initial stage (named as II in Fig. 1a, thereinafter) when O_3 was introduced into the chamber, BC particle did not show any change. However, after NH_3 and NO_2 were simultaneously introduced into the chamber (named as III in Fig. 1a, thereinafter), NO_2 concentration decreased immediately to about 10 ppb and then increased slowly to 50 ppb, while NO sharply decreased from 1.5 to 0.2 ppb and then gradually increased to about 0.5 ppb after the exposure (Fig. 1a). The d_m and ρ_{eff} of the seeded BC particles did not change after the initial exposure of O_3 alone (i.e., the II stage, Fig. 1b) but increased quickly after exposed to NO_2 and NH_3; d_m increased from the initial diameter of 117 ± 1.31 to 385 ± 1.91 nm with an increase in ρ_{eff} from 1.04 ± 0.01 to 1.48 ± 0.07 g cm^{-3} (Fig. 1b), together with a strong NO_3^- signal detected by the AMS (Fig. 1c), suggesting a large amount of nitrate coating on the BC surface. Previous studies have reported that O_3 could react with NO_2 and produce NO_3 radicals (R1), which further reacts with NO_2 to form N_2O_5 (R2) (Wu et al., 2020b; Zhang et al., 2021). Then, N_2O_5 diffuses onto the BC surface and reacts with H_2O molecules by forming HNO_3 (R3, R4) (Galib and Limmer, 2021; Wu et al., 2021). In this study, the HNO_3 experienced a further neutralization with NH_3 on the BC surface (R5) (Wang et al., 2016; Wu et al., 2020a), resulting in the growth of BC seeds with an increasing d_m.

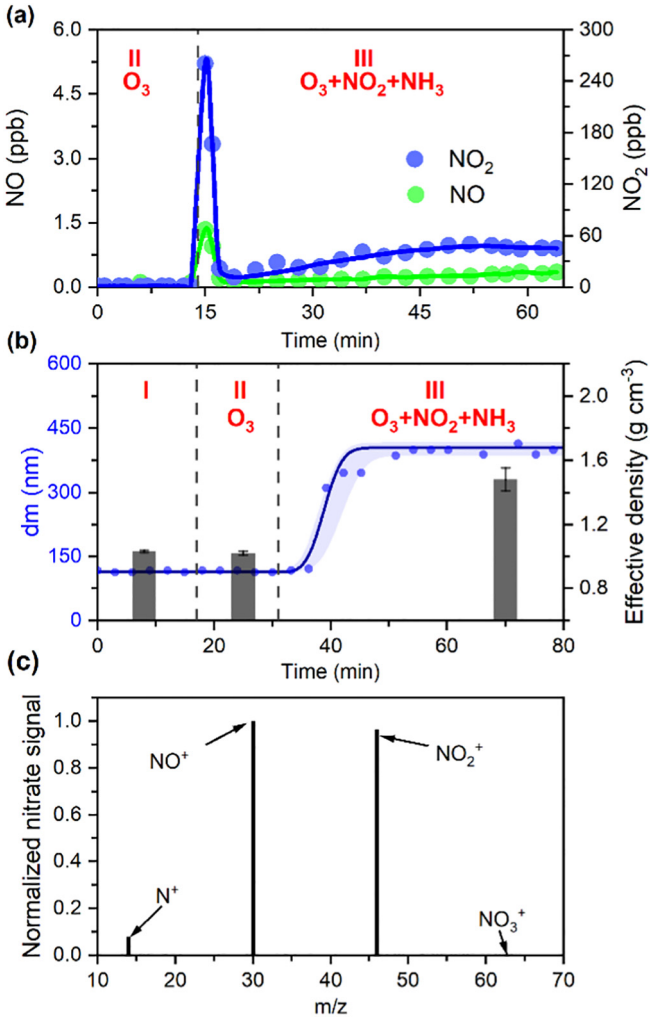

Fig. 1. Heterogeneous reaction of O_3 (300 ppb) and NO_2 (300 ppb) on BC surface under 75% RH conditions in the presence of NH_3 (500 ppb). (a) Concentrations of NO and NO_2 in the chamber as a function of the reaction time. (b) Time dependence of mobility diameter (d_m) and effective density (ρ_{eff}) of BC particles in the chamber during the consecutive exposure to O_3, NO_2 and NH_3. (c) HR-ToF-AMS spectra of nitrate ions from BC particles after the exposure.

$$NO_2(g) + O_3(g) \rightarrow NO_3(g) + O_2(g) \quad (1)$$

$$NO_2(g) + NO_3(g) \rightarrow N_2O_5(g) \quad (2)$$

$$N_2O_5(g) \rightarrow N_2O_5(ads) \quad (3)$$

$$N_2O_5(ads) + H_2O(ads) \rightarrow HNO_3(ads) \quad (4)$$

$$HNO_3(ads) + NH_3(ads) \rightarrow NH_4NO_3(ads) \quad (5)$$

$$N_2O_5(ads) + \{C\} \rightarrow N_2O_3(ads) + \{C \cdot O_2\} \quad (6)$$

$$N_2O_3(ads) \rightarrow NO(g) + NO_2(g) \quad (7)$$

Several researchers have investigated the uptake of N_2O_5 on soot and found that NO and NO_2 were the gas-phase product of the uptake (Karagulian and Rossi, 2007; Zelenov et al., 2016). Moreover, the decomposition of HNO_3 on BC surface also can produce NO and NO_2 (Disselkamp et al., 2000; Kleffmann and Wiesen, 2005). For the reaction of BC with nitric acid at 55% RH, Kleffmann and Wiesen (2005) and Choi and Leu (1998) found that only reversible adsorption was observed for nitric acid with a mixing ratio less than 600 ppbv and NO and NO_2 were formed as products only for nitric acid mixing ratios > 800 ppbv or at 503 K. Because the experiments here were performed under 298 K conditions and the AMS results showed that nitrate on the BC surface was completely neutralized with NH_3 as NH_4NO_3, the HNO_3 decomposition could be ruled out. Therefore, we believed that the uptake of N_2O_5 on the BC surface could generate NO_2 and NO through the reactions of R6 and R7, and then NO was further oxidized to NO_2 by O_3, resulting in the slight increases of NO_2 and NO in the chamber.

3.2. Chemical modification of BC by O_3 and NO_2

In this study, we used two parameters, i.e., D_m and ρ_{eff}, to characterize the change of BC particle morphology (Leung et al., 2017b; Schnitzler et al., 2014; Zhang et al., 2008). The D_m reflects the aging processes of BC particles, and the values of compact soot aggregates are often larger than those of lacy aggregates. The mass-mobility relationships of the seeded BC particles in the chamber before and after coating by NH_4NO_3 derived from the hydrolysis of N_2O_5 are shown in Fig. 2a. The initial particles had a D_m of 2.23 with an ρ_{eff} of 1.04 ± 0.01 g cm^{-3}. After 1 h of exposure to $NO_2/O_3/NH_3$, the D_m of BC particles increased to 2.94 with an ρ_{eff} of 1.48 ± 0.07 g cm^{-3}. TEM image shows that BC particles in the initial stage were chain-like but became spherical after the exposure (Fig. 2b and c), indicating that the coating of ammonium nitrate made the fractal, non-spherical BC aggregates restructure and condense to spherical

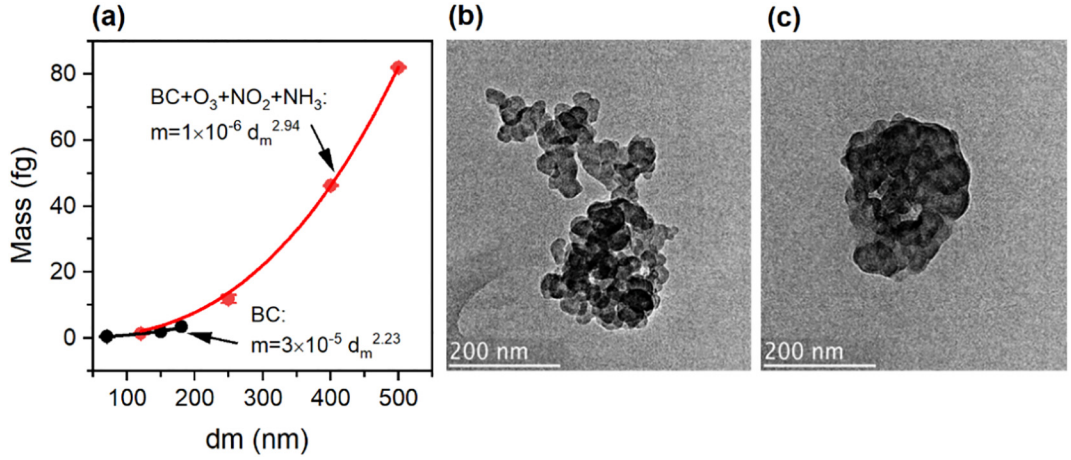

Fig. 2. Aging of BC during the exposure to O_3 (300 ppb), NO_2 (300 ppb) and NH_3 (500 ppb) under 75% RH conditions. (a) The dependence of BC mass on mobility diameter (d_m) before and after the exposure. (b) and (c) TEM image of BC particle before and after the exposure, respectively.

aggregates, which is in line with the previously published results (Yuan et al., 2019).

AMS mass spectra of the seeded BC particles before and after the exposures are shown in Fig. 3. Before the exposure, the seeded BC particle spectra displayed major signals only at m/z = 28 (CO^+) and m/z = 44 (CO_2^+), which are organic acid signatures (Hu et al., 2013), suggesting the occurrence of a small amount of carboxylic groups on the BC surface (Fig. 3a). After exposed to 300 ppb NO_2 for about 30 min, the BC particles displayed a mass spectrum pattern similar to that before the exposure (Fig. 3b), indicating the NO_2 alone cannot chemically modify BC surface because BC used in this work is chemically inert and NO_2 oxidation capacity is not strong enough. As shown in Fig. 3c, however, after exposed to O_3 alone, the intensity of m/z = 29 (CHO^+) and m/z = 43 ($C_2H_3O^+$) increased significantly, indicating that the BC surface was oxidized by O_3 and carbonyl groups were formed on the surface, which is mainly due to the stronger oxidation capacity of O_3 compared to NO_2 (Lambe et al., 2013; Peebles et al., 2011).

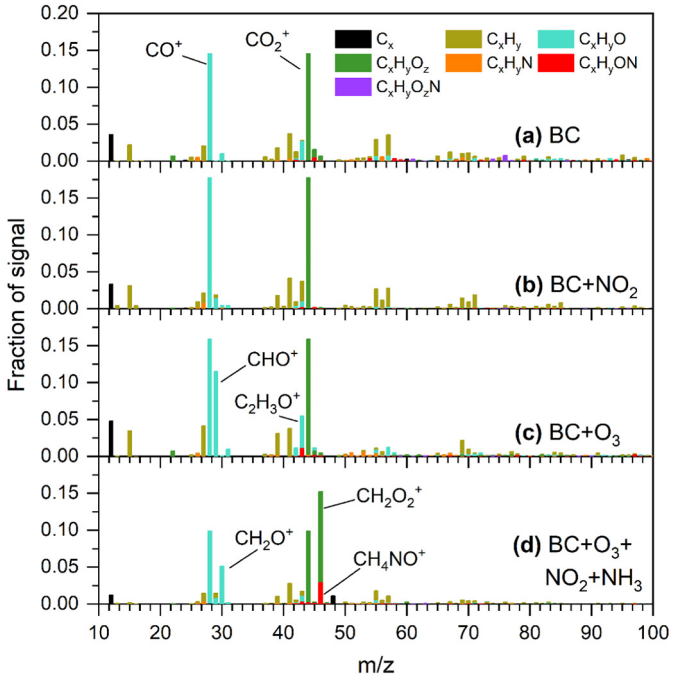

Fig. 3. HR-AMS mass spectra of seeded BC particles in the chamber. (a) Pure BC particles before the exposure. (b), (c) and (d) BC particles exposed to NO_2 (300 ppb), O_3 (300 ppb) and a mixture of NO_2 (300 ppb), O_3 (300 ppb) and NH_3 (500 ppb) for 1 h under 75% RH conditions, respectively.

Interestingly, we found that after exposed to the mixture of O_3, NO_2 and NH_3 the BC mass spectrum showed a notable change with a sharp increase in signal at m/z = 46 ($CH_2O_2^+$ and CH_4NO^+) and m/z = 30 (CH_2O^+) (Fig. 3d). The mass spectrum signals of the above oxygenated ions relative to the signal at m/z = 12, which is C^+ emitted from BC surface, are much stronger after the exposure to the O_3 and NO_2 mixture than those after the exposure to O_3 or NO_2 alone, indicating a strongly synergetic oxidizing effect of the two oxidants that significantly activated the BC surface by forming carbonyl, nitro and carboxylic groups.

3.3. Effect of RH on the reaction of NO_2 and O_3 on BC surface

Fig. 4 shows the changes in growth factor (GF: the ratio of the reaction steady-state d_m to the initial d_m) of the BC seeds after the exposure to NO_2, O_3 and NH_3 under various RH conditions. The d_m of seeded BC particles after the reaction increased from 117 ± 1.31 to 429 ± 1.87 nm when the RH increased from 30 ± 2% to 90 ± 2%, corresponding to an increase of the GF from 1.0 ± 0.05 to 3.5 ± 0.18, indicating that high RH is favorable for NH_4NO_3 formation. Assuming that all particles at the end of the reaction are core-shell structure, i.e., compact spheres with a BC core and an outer shell, the coating thicknesses (Δr_{me}) at the end of the reaction under various RH conditions can be estimated using the following formulas (III)–(V) (Peng et al., 2016).

$$d_{me} = \left(\frac{6m_p}{\pi\rho_m}\right)^{\frac{1}{3}} \quad \text{(III)}$$

$$\frac{m_p}{\rho_m} = \frac{m_{BC}}{\rho_{BC}} + \frac{(m_p - m_{BC})}{\rho_{NH4NO3}} \quad \text{(IV)}$$

$$\Delta r_{me} = \frac{1}{2}(d_{me,t} - d_{me,0}) \quad \text{(V)}$$

Where d_{me} is the mass equivalent diameter of BC particle ($d_{me,t}$ and $d_{me,0}$ is the d_{me} of fresh BC particle and aged BC particle, respectively); ρ_m is the material density of particle; ρ_{BC} is the material density of BC, 1.77 g cm^{-3} (Dalirian et al., 2018; Long et al., 2013); ρ_{NO3-} is the material density of NH_4NO_3, 1.72 g cm^{-3}.

As seen in Fig. 4a, the Δr_{me} increased from 2.0 ± 0.10 to 138 ± 6.93 nm as RH increased from 30 ± 2% to 90 ± 2%. Fig. 4b shows the time dependence of the amount of nitrate formed on per particle under various RH conditions, which agreed well with those of the GF and the coating thickness, indicating that the formation of NH_4NO_3 on the BC surface is dependent on the water adsorption. Previous studies found that water molecules can be trapped firstly on BC surface by hydrophilic chemical groups to form hydrogen bonds, or by confinement effects in small size of pores

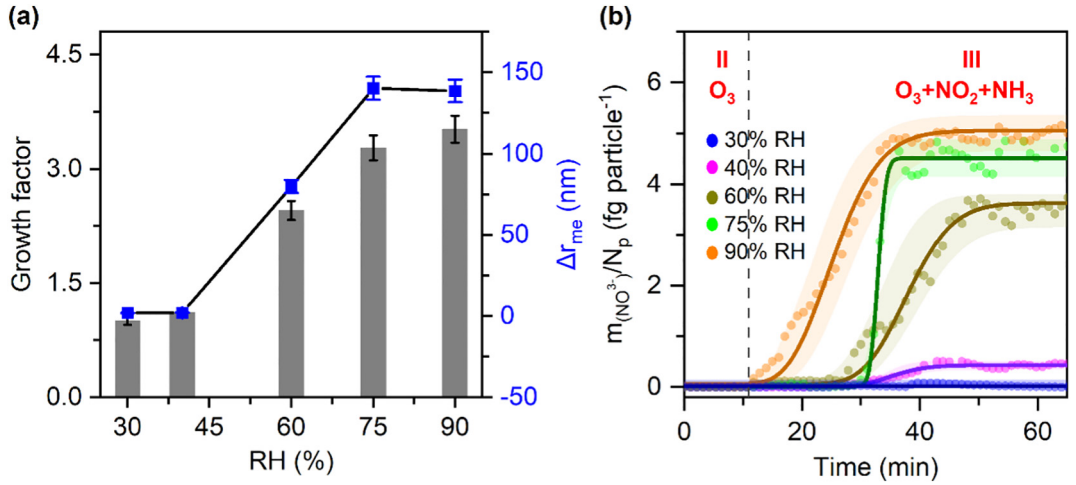

Fig. 4. Effect of relative humidity (RH) on BC aging. (a) The dependence of growth factor and coating thickness (Δrme) of BC on RH. (b) The formation amount of nitrate on individual BC particles in the chamber as a function of reaction time during the exposure of BC seeds to O_3 (300 ppb), NO_2 (300 ppb) and NH_3 (500 ppb) under different RH conditions ($m(NO_3^-)$ is the formation amount of nitrate on BC particle surface; Np is the particle number).

(Hantal et al., 2010; Seisel et al., 2004). Then, other water molecules were adsorbed on the surface mainly by the formation of H_2O-H_2O hydrogen bonds with the already adsorbed H_2O molecules (Hantal et al., 2010). Once a monolayer of water molecules is formed, further adsorption of water molecules can occur in the micropores of BC, and finally forming a multilayer adsorption at RH above 80% (Seisel et al., 2005). In this work, regal black R400 was used as the seed particle, which contains a certain amount of organic acid groups on the surface. In addition, the graphitic surface can be further oxidized by O_3 to produce additional hydrophilic oxygen-containing functional groups. At low RH, water molecules can be trapped by those hydrophilic groups on the BC surface via chemisorption or confinement effect. Thus, N_2O_5 adsorbed can react with water molecules to form HNO_3 on the BC surface. The amount of water molecules adsorbed on the BC surface increased with the increasing of RH from 30 ± 2% to 75 ± 2%, so the amount of nitrate also increased with the increasing RH.

As shown in Fig. 4b, under lower RH conditions, i.e., < 75 ± 2%, a rapid formation of nitrate on the BC cannot be observed until NO_2 was introduced into the chamber for about 20 min. However, after NO_2 was introduced the rapid formation of nitrate in the chamber can be instantly observed when RH was 90 ± 2%. Under the lower RH conditions the water molecules adsorbed on the BC surface is monolayer and the amount adsorbed is dependent on the amount of the BC surface active sites, i.e., hydrophilic groups. Due to the limited number of hydrophilic groups on the BC surface, only a few water molecules can be absorbed on the BC surface. Thus, N_2O_5 molecules must diffuse onto the specific sites of BC micropore surface where water molecules are available and then can react with the water molecules to form nitrate. Such a diffusing process is slow and time consuming. In contrast, under 90 ± 2% RH conditions, multilayer water molecules were absorbed on the surface and in the micropores of BC particles, which enabled N_2O_5 to hydrolyze directly on the aqueous phase with no diffusion, resulting in the rapid formation of nitrate without any delay.

3.4. Impact of KCl on the O_3 and NO_2 reaction on BC

To mimic the atmospheric aging process of BC emitted from biomass combustion, KCl-treated BC particles with a 130 nm dry diameter were introduced into the chamber. As seen in Fig. S2, the exponent (2.41) of the KCl-treated BC particles was larger than the value of pure BC particles (2.23) (Fig. 2a), indicating the particles was a little bit of more compact than the pure BC particles. As shown in Fig. 5, besides C and O elements, K and Cl elements were also observed at the same location, indicating an even distribution of KCl microcrystals in the BC particles.

To investigate the role of KCl during the heterogeneous formation process of nitrate on BC surface, the KCl-treated BC particles were exposed consecutively to O_3 (300 ppb), NO_2 (300 ppb) and NH_3 (500 ppb) for 1 h under low (40 ± 2%) and high (75 ± 2%) RH, respectively. As seen in Fig. 6a, after NO_2 and NH_3 were injected into the chamber, the d_m of the KCl-treated BC particles increased from 131 ± 1.37 to 163 ± 1.41 nm with a GF of 1.24 ± 0.06 under 40% RH conditions and to 414 ± 1.63 nm with a GF of 3.6 ± 0.18 under 75 ± 2% RH conditions, respectively, suggesting the formation amount of nitrate under 40% RH was much lower than that under 75 ± 2% RH conditions. As shown in Fig. 6a, after the exposure for about 60 min, the d_m become constant, indicating that nitrate amount on the KCl-treated BC particles was saturated. It can be seen from Fig. 6b, at this moment the nitrate amount under 40 ± 2% RH and 75 ± 2% RH were 0.53 and 6.8 f. per particle, respectively, which are about 50% higher than those for pure BC seeds, indicating an enhancing role of KCl in the nitrate formation on BC surface. KCl is hygroscopic and can increases the amount of water molecules absorbed by the seeded BC particles, thus, promoting the conversion of N_2O_5 to nitrate. Moreover, N_2O_5 can react with Cl ions and form KNO_3 on the surface of mixed particles (R8), which is also hygroscopic and further promotes more nitrate formed on the mixed particle surface (Ahern et al., 2018; Tham et al., 2018).

$$N_2O_5 + KCl \rightarrow KNO_3 + ClNO_2 \quad (8)$$

In the reaction process, particle surface properties mainly affect the initial reaction stage, instead of the rapidly formation stage of nitrate, which is caused by the reaction of N_2O_5 with multilayer adsorption water. To further explore the impact of KCl on the BC aging process, we calculated the nitrate formation rate on the seed surface before the rapid growth stage, which was a ~ 20 min slow growth stage after NO_2 and NH_3 were introduced into the chamber (Figs. 4 and 6). As shown in Table 1, in the 20 min of the reaction, the nitrate formation rates on KCl-treated BC particles under 40 ± 2% RH and 75 ± 2% RH were 3–4 times larger than those on the pure BC particle, which can be ascribed to the hygroscopicity of KCl. In addition, several researches have proved that the heterogeneous reaction of N_2O_5 with Cl^- in Cl^--containing droplets is faster than the diffusion of N_2O_5 in water (Royer et al., 2021; Zhang et al., 2021), which is also possibly responsible for the faster formation rate of nitrate on the KCl-treated seeds.

4. Conclusion

This study investigated the heterogeneous formation process of nitrate on BC surface through reaction of O_3 with NO_2 under different RH conditions in the presence of NH_3. The results showed that N_2O_5 formed by reaction of O_3 and NO_2 can quickly hydrolyze into HNO_3 and subsequently

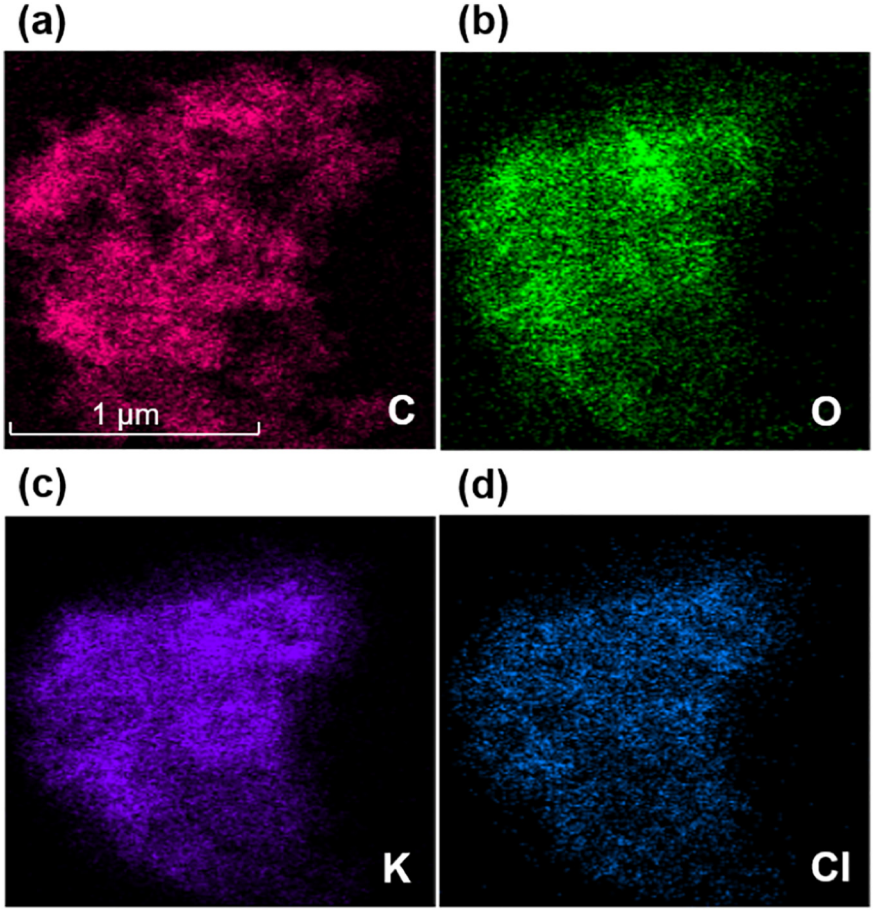

Fig. 5. Elemental mapping of KCl-treated BC particles collected from the chamber. C, O, K, Cl mapping were shown in (a), (b), (c), (d), respectively.

neutralized by NH_3 to form NH_4NO_3 on the BC surface, along with a slight decomposition of N_2O_5 to NO and NO_2. NH_4NO_3 coating on the BC surface led to the chain-like BC aggregates restructure and condense to spherical aggregates. The AMS analysis results further showed that ozone and nitrogen dioxide mixture exhibited a strongly synergistic oxidizing effect that can significantly activate BC surface by forming carbonyl, nitro and carboxylic groups, which were favorable for the absorption of water vapor onto the BC surface and enhanced the NH_4NO_3 formation. Under <75 ± 2% RH conditions only a small amount of water molecules can be adsorbed by the activated BC surface as a monolayer format, thus the NH_4NO_3 coating process consists of two phases, i.e., a diffusing of N_2O_5 onto the BC micropore surface and a subsequent hydrolysis. In contrast, under 90 ± 2% RH conditions, due to a multilayer of water molecules formed on the BC surface, N_2O_5 can directly hydrolyze on the aqueous phase, causing a rapid coating of NH_4NO_3. The coating rate of NH_4NO_3 on KCl-treated BC particles at the initial stage was 3–4 times higher than that on the pure

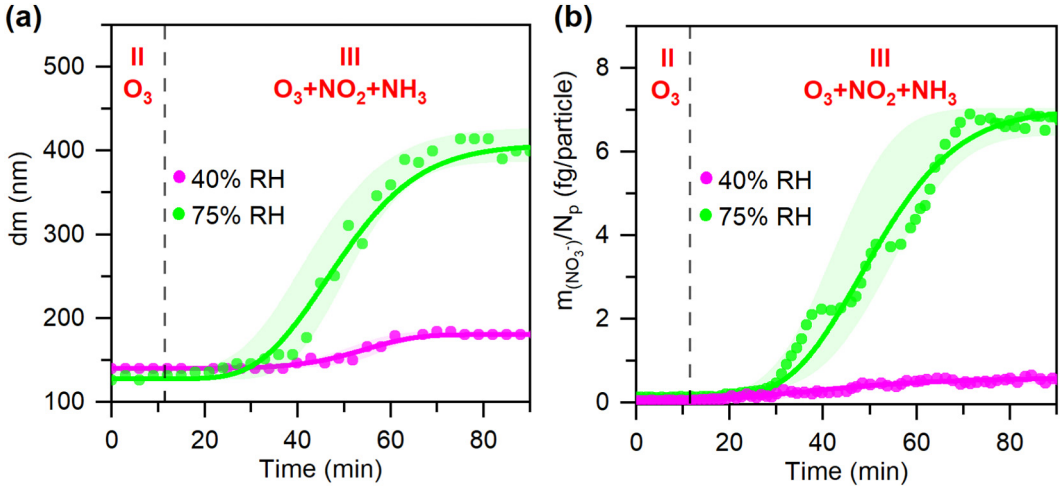

Fig. 6. Aging process of KCl-treated BC in the chamber during the consecutive exposure to O_3 (300 ppb), NO_2 (300 ppb) and NH_3 (500 ppb). (a) Variations in mobility diameter (d_m) of KCl-treated BC particles. (b) The formation amount of nitrate on individual KCl-treated BC particles ($m(NO_3^-)$ is the formation amount of nitrate on KCl-treated BC particle surface; Np is the particle number).

Table 1
A comparison on the formation rate of nitrate on per particles in the initial 20 min under two RH conditions.

RH/%	Seed	NO_3^- (fg)	Formation rate (fg min^{-1})
40	BC	0.079	0.0088
75		0.14	0.016
40	KCl-treated BC	0.31	0.034
75		0.46	0.051

BC particles, along with a 50% increase in the coating amount at the end of the reaction, indicating an enhanced formation of NH_4NO_3 on the surface, which is mainly due to the salt hygroscopic property.

The BC seeds (Regal 400) used in this study are pure and chemically inert due to the very low level of organics on the surface. However, BC particles produced in the combustion process are much more chemically active and hygroscopic as they are often coated with abundant organic compounds and inorganic salts. Thus, the dynamic parameters such as growth factor and nitrate formation rate obtained by this work are only representative of the lower limits of reactivity of real BC particles in the atmosphere. Moreover, this study was conducted under dark conditions and solar radiation effects are not considered. Thus, in the future it is necessary to study the heterogeneous reaction of NO_2 and O_3 on the surface of BC particles directly emitted from the combustion process without any pre-treatment with a consideration on the solar radiation effects.

CRediT authorship contribution statement

GW designed the experiment and supervised the research; SZ, XX and DL performed the experiment; SZ and GW conducted the data analysis and wrote the paper. YL, YW, SL and SG contributed to the paper with useful scientific discussions or comments.

Declaration of competing interest

We declare that we have no known competing financial interests or personal relationships that could have appeared to influence the work reported in this paper.

Acknowledgements

This work was financially supported by National Natural Science Foundation of China (No. 42130704, 41807355), the Shanghai Science and Technology Innovation Action Plan (No. 20dz1204011), and the program of Institute of Eco-Chongming and ECNU Happiness Flower.

Appendix A. Supplementary data

Supplementary data to this article can be found online at https://doi.org/10.1016/j.scitotenv.2022.153649.

References

Ahern, A.T., Goldberger, L., Jahl, L., et al., 2018. Production of N_2O_5 and $ClNO_2$ through nocturnal processing of biomass-burning aerosol. Environ. Sci. Technol. 52, 550–559.
Ban-Weiss, G.A., Lunden, M.M., Kirchstetter, T.W., et al., 2009. Measurement of black carbon and particle number emission factors from individual heavy-duty trucks. Environ. Sci. Technol. 43, 1419–1424.
Choi, W., Leu, M.-T., 1998. Nitric acid uptake and decomposition on black carbon (soot) surfaces: its implications for the upper troposphere and lower stratosphere. J. Phys. Chem. A 102, 7618–7630.
Dalirian, M., Ylisirniö, A., Buchholz, A., et al., 2018. Cloud droplet activation of black carbon particles coated with organic compounds of varying solubility. Atmos. Chem. Phys. 18, 12477–12489.
Disselkamp, R.S., Carpenter, M.A., Cowin, J.P., 2000. A chamber investigation of nitric acid-soot aerosol chemistry at 298 K. J. Atmos. Chem. 37, 113–123.
Galib, M., Limmer, D.T., 2021. Reactive uptake of N_2O_5 by atmospheric aerosol is dominated by interfacial processes. Science 371, 921–925.
Ge, S., Wang, G., Zhang, S., et al., 2019. Abundant NH_3 in China enhances atmospheric HONO production by promoting the heterogeneous reaction of SO_2 with NO_2. Environ. Sci. Technol. 53, 14339–14347.
Guan, C., Li, X., Zhang, W., et al., 2017. Identification of nitration products during heterogeneous reaction of NO_2 on soot in the dark and under simulated sunlight. J. Phys. Chem. A 121, 482–492.
Hantal, G., Picaud, S., Hoang, P.N., et al., 2010. Water adsorption isotherms on porous onionlike carbonaceous particles. Simulations with the grand canonical Monte Carlo method. J. Chem. Phys. 133, 144702.
He, C., Liou, K.N., Takano, Y., et al., 2015. Variation of the radiative properties during black carbon aging: theoretical and experimental intercomparison. Atmos. Chem. Phys. 15, 11967–11980.
Hoesly, R.M., Smith, S.J., Feng, L., et al., 2018. Historical (1750–2014) anthropogenic emissions of reactive gases and aerosols from the community emissions data system (CEDS). Geosci. Model Dev. 11, 369–408.
Hu, W.W., Hu, M., Yuan, B., et al., 2013. Insights on organic aerosol aging and the influence of coal combustion at a regional receptor site of central eastern China. Atmos. Chem. Phys. 13, 10095–10112.
IPCC, 2013. Summary for policymakers. In: Stocker, T.F., Qin, D., Plattner, G.-K., et al. (Eds.), Climate Change 2013: The Physical Science Basis. Contribution of Working Group I to the Fifth Assessment Report of the Intergovernmental Panel on Climate Change. Cambridge University Press, Cambridge, United Kingdom and New York, NY, USA 2216 pp.
Jiang, H., Liu, Y., Xie, Y., et al., 2019. Oxidation potential reduction of carbon nanomaterials during atmospheric-relevant aging: role of surface coating. Environ. Sci. Technol. 53, 10454–10461.
Karagulian, F., Rossi, M.J., 2007. Heterogeneous chemistry of the NO_3 free radical and N_2O_5 on decane flame soot at ambient temperature: reaction products and kinetics. J. Phys. Chem. A 111, 1914–1926.
Kleffmann, J., Wiesen, P., 2005. Heterogeneous conversion of NO_2 and NO on HNO_3 treated soot surfaces: atmospheric implications. Atmos. Chem. Phys. 5, 77–83.
Lambe, A.T., Cappa, C.D., Massoli, P., et al., 2013. Relationship between oxidation level and optical properties of secondary organic aerosol. Environ. Sci. Technol. 47, 6349–6357.
Leung, K.K., Schnitzler, E.G., Jäger, W., et al., 2017a. Relative humidity dependence of soot aggregate restructuring induced by secondary organic aerosol: effects of water on coating viscosity andsurface tension. Environ. Sci. Technol. Lett. 4, 386–390.
Leung, K.K., Schnitzler, E.G., Dastanpour, R., et al., 2017b. Relationship between coating-induced soot aggregate restructuring and primary particle number. Environ. Sci. Technol. 51, 8376–8383.
Li, K., Jacob, D.J., Liao, H., et al., 2019. Anthropogenic drivers of 2013–2017 trends in summer surface ozone in China. Proc. Natl. Acad. Sci. U. S. A. 116, 422–427.
Li, W., Liu, L., Zhang, J., et al., 2021. Microscopic evidence for phase separation of organic species and inorganic salts in fine ambient aerosol particles. Environ. Sci. Technol. 55, 2234–2242.
Liao, H., Shang, J., 2015. Regional warming by black carbon and tropospheric ozone: a review of progresses and research challenges in China. J. Meteorol. Res. 29, 525–545.
Long, C.M., Nascarella, M.A., Valberg, P.A., 2013. Carbon black vs. Black carbon and other airborne materials containing elemental carbon: physical and chemical distinctions. Environ. Pollut. 181, 271–286.
Longfellow, C.A., Ravishankara, A.R., Hanson, D.R., 2000. Reactive and nonreactive uptake on hydrocarbon soot: HNO3, O3, and N2O5. J. Geophys. Res. Atmos. 105, 24345–24350.
Nie, B., Peng, C., Wang, K., et al., 2020. Structure and formation mechanism of methane explosion soot. ACS Omega 5, 31716–31723.
Peebles, B.C., Dutta, P.K., Waldman, W.J., et al., 2011. Physicochemical and toxicological properties of commercial carbon blacks modified by reaction with ozone. Environ. Sci. Technol. 45, 10668–10675.
Peng, J., Hu, M., Guo, S., et al., 2016. Markedly enhanced absorption and direct radiative forcing of black carbon under polluted urban environments. Proc. Natl. Acad. Sci. U. S. A. 113, 4266–4271.
Royer, H.M., Mitroo, D., Hayes, S.M., et al., 2021. The role of hydrates, competing chemical constituents, and surface composition on $ClNO_2$ formation. Environ. Sci. Technol. 55, 2869–2877.
Saathoff, H., Naumann, K.H., Riemer, N., et al., 2001. The loss of NO_2, HNO_3, NO_3/N_2O_5, and HO2/HOONO2on soot aerosol: a chamber and modeling study. Geophys. Res. Lett. 28, 1957–1960.
Schnitzler, E.G., Dutt, A., Charbonneau, A.M., et al., 2014. Soot aggregate restructuring due to coatings of secondary organic aerosol derived from aromatic precursors. Environ. Sci. Technol. 48, 14309–14316.
Seisel, S., Lian, Y., Keil, T., et al., 2004. Kinetics of the interaction of water vapour with mineral dust and soot surfaces at T = 298 K. Phys. Chem. Chem. Phys. 6, 1926–1932.
Seisel, S., Pashkova, A., Lian, Y., et al., 2005. Water uptake on mineral dust and soot: a fundamental view of the hydrophilicity of atmospheric particles? Faraday Discuss. 130, 437–451 discussion 491-517, 519-24.
Tham, Y.J., Wang, Z., Li, Q., et al., 2018. Heterogeneous N_2O_5 uptake coefficient and production yield of ClNO2 in polluted northern China: roles of aerosol water content and chemical composition. Atmos. Chem. Phys. 18, 13155–13171.
Wang, R., Tao, S., Wang, W., et al., 2012. Black carbon emissions in China from 1949 to 2050. Environ. Sci. Technol. 46, 7595–7603.
Wang, G., Zhang, R., Gomez, M.E., et al., 2016. Persistent sulfate formation from London fog to Chinese haze. Proc. Natl. Acad. Sci. U. S. A. 113, 13630–13635.
Wang, J.Y., Wang, G.H., Wu, C., et al., 2020. Enhanced aqueous-phase formation of secondary organic aerosols due to the regional biomass burning over North China plain. Environ. Pollut. 256.
Wei, X., Zhu, Y., Hu, J., et al., 2020. Recent progress in impacts of mixing state on optical properties of black carbon aerosol. Curr. Pollut. Rep. 6, 380–398.
Wu, C., Wang, G.H., Cao, C., et al., 2019. Chemical characteristics of airborne particles in Xi'an, inland China during dust storm episodes: implications for heterogeneous formation of ammonium nitrate and enhancement of N-deposition. Environ. Pollut. 244, 877–884.

Wu, C., Wang, G.H., Li, J., et al., 2020a. Non-agricultural sources dominate the atmospheric NH3 in Xi'an, a megacity in the semi-arid region of China. Sci. Total Environ. 722.
Wu, C., Zhang, S., Wang, G., et al., 2020b. Efficient heterogeneous formation of ammonium nitrate on the saline mineral particle surface in the atmosphere of East Asia during dust storm periods. Environ. Sci. Technol. 54, 15622–15630.
Wu, C., Liu, L., Wang, G.H., et al., 2021. Important contribution of N_2O_5 hydrolysis to the daytime nitrate in Xi' an, China during haze periods: Isotopic analysis and WRF-Chem model simulation. Environmental Pollution 288.
Yuan, Q., Xu, J., Wang, Y., et al., 2019. Mixing state and fractal dimension of soot particles at a remote site in the southeastern Tibetan Plateau. Environ. Sci. Technol. 53, 8227–8234.
Zelenov, V.V., Aparina, E.V., Kashtanov, S.A., et al., 2016. Kinetics of N_2O_5 uptake on a methane soot coating. Russ. J. Phys. Chem. B 10, 341–352.
Zhang, R., Khalizov, A.F., Pagels, J., et al., 2008. Variability in morphology, hygroscopicity, and optical properties of soot aerosols during atmospheric processing. Proc. Natl. Acad. Sci. U. S. A. 105, 10291–10296.
Zhang, F., Wang, Y., Peng, J., et al., 2020a. An unexpected catalyst dominates formation and radiative forcing of regional haze. Proc. Natl. Acad. Sci. U. S. A. 117, 3960–3966.
Zhang, Y., Vu, T.V., Sun, J., et al., 2020b. Significant changes in chemistry of fine particles in wintertime Beijing from 2007 to 2017: impact of clean air actions. Environ. Sci. Technol. 54, 1344–1352.
Zhang, S., Li, D., Ge, S., et al., 2021. Rapid sulfate formation from synergetic oxidation of SO_2 by O_3 and NO_2 under ammonia-rich conditions: implications for the explosive growth of atmospheric PM2.5 during haze events in China. Sci. Total Environ. 772.